American Mineralogist, Volume 91, pages 1230–1239, 2006

Site preference and local geometry of Sc in garnets: Part I. Multifarious mechanisms in the pyrope-grossular join

Roberta Oberti,[1] Simona Quartieri,[2,*] Maria Chiara Dalconi,[2,†] Federico Boscherini,[3] Gianluca Iezzi,[4] Massimo Boiocchi,[5] and Sigrid Griet Eeckhout[6]

[1]CNR, Istituto di Geoscienze e Georisorse, Università di Pavia, via Ferrata 1, I-27100 Pavia, Italy
[2]Dipartimento di Scienze della Terra,Università di Messina, Salita Sperone 31, I-98166 Messina S. Agata, Italy
[3]Dipartimento di Fisica and CNISM, Università di Bologna, Viale Berti Pichat 6/2, I-40127 Bologna, Italy
[4]Dipartimento di Scienze della Terra, Università di Chieti, via dei Vestini 30, I-66013 Chieti Scalo, Italy
[5]Centro Grandi Strumenti, Università di Pavia, via Bassi 21, I-27100 Pavia, Italy
[6]European Synchrotron Radiation Facility, 6 rue Jules Horowitz, BP 220, F-38043 Grenoble Cedex, France

Abstract

We applied different independent techniques (electron microprobe analysis, structure refinement, and X-ray absorption spectroscopy) to unravel the possible mechanisms of Sc incorporation in the pyrope-grossular join. Samples were synthesized at elevated pressure and temperature by adding 5 wt% of Sc_2O_3 to selected nominal compositions (pyrope, $pyrope_{60}grossular_{40}$, $pyrope_{20}grossular_{80}$, and grossular). In this way, the site of incorporation was not pre-determined, and only depends on the availability of a mechanism for local charge-balance. The EXAFS spectra of the two end-members could be analyzed by a multi-shell fit procedure, whereas the chemical heterogeneity of the Sc-doped solid-solution terms prevented this approach. However, the available information allows detection of different mechanisms of incorporation, which are active as a function of the bulk composition. In pyrope, Sc mainly enters the dodecahedral X site, and the local charge balance is achieved by incorporation of Mg at the adjacent tetrahedral Z site. Local charge-balance requirements suggest that a Z site occupied by Mg bridges two X sites occupied by Sc. When the entrance of Ca provides relaxation of the averaged structure, Sc may enter all the three available cation sites via the coupled heterovalent exchange $^{X}Sc_1{}^{Z}Sc_1{}^{X}Mg_{-1}{}^{Z}Si_{-1}$ and the homovalent exchange $^{Y}Sc_1{}^{Y}Al_{-1}$. In the samples of this work, there is an apparent limit in the Sc incorporation at the Y site, which is in contrast to the favored mechanism of incorporation in Sc-doped andradites. This limit can be explained in terms of relative dimensions of the structural sites when Al is the dominant Y cation. These results must be taken into account when evaluating trace-element behavior in garnets for geochemical purposes. In particular, they explain why D_{Sc} can be treated together with D_{REE} in models based on the elastic strain theory in garnets close to the pyrope composition, but deviate from the parabolic fit in grossular-rich garnets.

Keywords: Crystal structure, garnet, trace elements and REE, scandium, XAS, XRD data, crystal synthesis

Introduction

Trace-elements behavior is a fundamental tool in petrogenetic studies, and is generally used to decipher the sequence of processes, which modified the composition of the crystalline and co-existing liquid (fluid or melt) phases. Models of trace-elements behavior are mainly obtained via a method based on the elastic-strain theory, where the available experimental mineral/melt partition coefficients (*D*) of series of homovalent cations occurring at the same (group of) structural sites are treated in terms of pseudo-parabolic trends (Brice 1975; Blundy and Wood 1994). These parabolae have a vertex that corresponds to the "ideal" cation whose radius (r_0) best fits the dimension of the site and does not generate any strain, and a width inversely proportional to the effective Young's modulus of the site (*E*). This approach is capable of correctly interpreting and predicting trace element partitioning when (1) the site preference and coordination for each trace element is known and (2) accurate models are available for site partitioning, and thus for the different crystal-chemical mechanisms of incorporation occurring as a function of changes in pressure (*P*), temperature (*T*), and chemistry (*X*) of the system.

Scandium is an interesting element in this regard, because it is a transition element with a unique ionic charge. It can thus be used as an indicator of the behavior of the other transition elements for which the interpretation of measured partition coefficients (*D*) is troublesome because of the presence of different oxidation states. Moreover, Sc (with $^{[8]}r = 0.87$ Å and $^{[6]}r = 0.745$ Å; all the *r* values in this paper are from Shannon 1976) is the smallest among the cations possibly entering the dodecahedral X site (Fig. 1), but the largest among those possibly occurring at the octahedral Y sites, such as Al ($^{[6]}r$ = 0.535 Å), Cr ($^{[6]}r$ = 0.615 Å), and Mn^{3+} and Fe^{3+} ($^{[6]}r = 0.645$ Å). This means that the predicted values of r_0 and *E*, are strongly influenced by whether

* E-mail: simonaq@unimo.it
† Present address: Dipartimento di Scienze della Terra, Università di Ferrara, via Saragat 1, I-44100 Ferrara, Italy

0003-004X/06/0809–1230$05.00/DOI: 10.2138/am.2006.2037

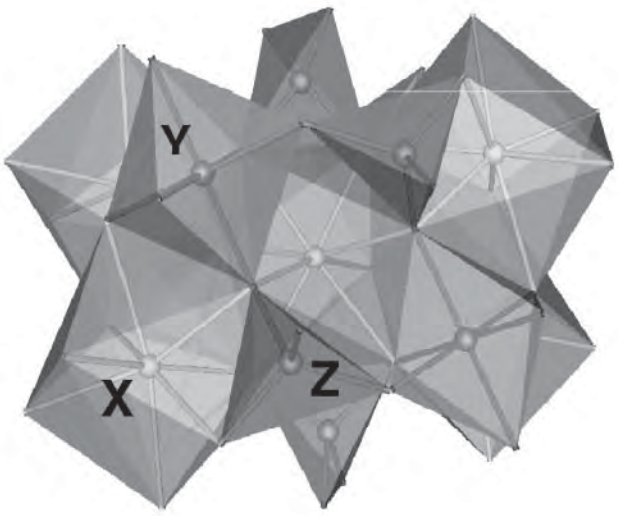

FIGURE 1. Details of the garnet structure, showing the connection between tetrahedra (Z), octahedra (Y), and dodecahedra (X).

Sc substitutes at one site or another, with possible implications also on the interpretation of D_{REE}. Therefore, different partitioning systematics may be inferred as a function of the bulk composition.

Much work has been done to interpret the garnet-melt partition coefficients measured for trivalent trace-elements in garnets, especially in the pyrope-grossular (prp-grs) join because these garnets are crucial for petrogenetic studies in igneous and subduction environments (van Westrenen et al. 1999, 2000, 2001, 2003), and because this solid solution shows large non-idealities in both structural and geochemical behavior. In particular, the garnet-melt partitioning experiments reported in van Westrenen et al. (1999) showed that, at P = 3 GPa and T = 1545 °C, Sc is always compatible from prp_9grs_{91} to $prp_{84}grs_{16}$, and that the D_{Sc} values double with increasing grs content. D_{Sc} values fall close to the crystal lattice strain fit for trivalent cations at the X site in pyrope-rich compositions, but are higher than those predicted for grossular-rich compositions. Thus these authors suggested that Sc may partition between the X and Y sites in these compositions. The atomistic simulations reported in van Westrenen et al. (2003) yielded the incorporation of Sc and Li into two adjacent X polyhedra as the energetically favored (defect) configuration. Unfortunately, this hypothesis could not be verified in the present work, as the reagents do not contain Li (or Na).

Albeit these recent hints, so far there is no direct evidence for the presence of Sc in multiple sites in the garnet structure, and Sc is generally considered in diadochy with Al and Fe^{3+} since the pioneering work of Ito and Frondel (1968).

Long-range information on Sc coordination in garnets is available only for the composition $Ca_3Sc_2Si_3O_{12}$ (Mill et al. 1977), where Sc is octahedrally coordinated. Experimental work at 1 bar and 2 GPa has shown complete solid solution between andradite (adr, $Ca_3Fe_2Si_3O_{12}$) and $Ca_3Sc_2Si_3O_{12}$ garnet, with essentially ideal volumes of mixing (Woodland and Angel 1996a, 1996b). However, Mössbauer analysis of the syntheses done at 1 bar showed that some Fe^{3+} occurs at the tetrahedral Z site, thus implying partitioning of Sc between the X and the Y sites (Woodland and Angel 1996a, 1996b). Information on Sc incorporation in andraditic garnets will be provided and discussed in the companion paper (Quartieri et al. 2006).

In this paper, we report on the multifarious behavior observed for Sc in synthetic compositions along the pyrope-grossular join. This issue was addressed combining accurate chemical and structural characterization of synthetic products, doped by minor Sc, and X-ray Absorption Spectroscopy (XAS) analysis and simulation of the measured spectra, following a method successfully used for Yb, Nd, Ce, Dy, and Ca (Quartieri et al. 1999a, 1999b, 2002, 2004; Oberti et al. 2006).

EXPERIMENTAL DETAILS

Synthesis

The aim of this work is to allow recognition of the different mechanisms of incorporation for Sc; therefore, we prepared the starting products according to the selected stoichiometries (prp, $prp_{60}grs_{40}$, $prp_{20}grs_{80}$, grs) and then added to these mixtures 5 wt% of Sc_2O_3 (99.9%) in excess. The composition of the two solid solution terms were chosen based on the available crystal-chemical knowledge of the prp-grs join, which shows a structural instability between $prp_{50}grs_{50}$ and $prp_{35}grs_{65}$, and frequent sample heterogeneity (mixtures) around $prp_{50}grs_{50}$. We used high-purity (99.99%) MgO, $CaCO_3$, Al_2O_3, and SiO_2 commercial reagents, which were dried overnight at 150 °C. The mixtures were then slowly de-carbonated at 1000 °C for several hours in a furnace. The agreement between calculated and measured CO_2 weight loss was used to check the chemical quality of the starting materials. All the synthesis experiments were done with an end-loaded 0.5 inch piston cylinder apparatus installed at the Bayerisches Geoinstitut, using the classical *hot piston-in* technique and working at 1000 °C and 3 GPa for 24 hours. The starting materials were sealed in cylindrical Pt capsules (length: 10 mm, external diameter: 5 mm, capsule thickness: 1 mm) after adding 20 wt% of bi-distilled water. The Pt capsules were placed inside pyrophyllite sample holders, and inserted in cylindrical tapered graphite furnaces used to attain high temperature. The talc-pyrex assemblage, mantled by a lead foil, was used as pressure medium, with an accuracy (friction corrected) of about ±0.05 GPa. The temperature of syntheses was continuously monitored by $Pt\text{-}Pt_{90}Rh_{10}$ thermocouples, placed about 2 mm from the top of the sample charge, and separated from it with an alumina disk; the estimated accuracy is ±10 °C. At the end of the run isobaric quenching was achieved by switching the power supply off, resulting in a cooling time from set point temperature down to 500 °C of less than 10 s.

The obtained run-products were first checked by XRPD and SEM-EDS analyses (see below) and then used for a new series of syntheses following the "recycling" strategy proposed by Ganguly et al. (1993) to improve the chemical homogeneity of the garnet products. These authors showed that the chemical homogeneity can be confidentally evaluated from the separation of the XRPD (Cu) $K\alpha_1$ and $K\alpha_2$ doublets at 2θ angles higher than 50° (spatial resolution is directly related to homogeneity). Sc-doped pyrope has several well-resolved intense XRPD $K\alpha_1$ and $K\alpha_2$ doublets, and Sc-doped grossular has less resolved doublets. The two intermediate nominal compositions have very badly resolved $K\alpha_1$ and $K\alpha_2$ doublets at high 2θ angles.

The run-products synthesized at 1000 °C were carefully ground, mixed with about 25 wt% of the starting oxide mixtures, and used as starting materials for a second set of experiments. These new starting mixtures (75 wt% of ground crystalline materials plus 25 wt% of oxide starting materials) were sealed in Pt capsules (same dimensions as before), and 2 wt% of distilled water was added to improve the kinetics of crystallization. The recycling runs were carried out for 24 hours at 1100 °C and 4 GPa. Note that Ganguly et al. (1993) did recycling at much higher T conditions (1400 °C), which could not be attained in this work. XRPD analysis of these recycled run products yielded an improved resolution of the $K\alpha_1$ and $K\alpha_2$ Bragg reflection doublets for all four nominal garnet compositions. In particular, Sc-doped pyrope had excellent chemical homogeneity, better than Sc-doped grossular. The two intermediate samples ($prp_{60}grs_{40}$, $prp_{20}grs_{80}$) still had a poor resolution of the $K\alpha_1$ and $K\alpha_2$ Bragg reflection doublets collected at higher 2θ angles.

The crystal size is strongly dependent on the garnet compositions: Sc-doped pyrope may reach 1 mm, Sc-doped grossular rarely exceeds 50 μm, and the intermediate compositions are typically between 5 and 20 μm.

SEM and EMPA analysis

For the synthetic samples, SEM-EDS inspections were carried out with a Leo-Gemini scanning electron microscope equipped with an Oxford EDAX detector; the

SEM analysis was done on carbon coated thin sections where mg-size samples of crushed and polished run-products had been mounted. Electron microprobe (EMP) analysis was performed using a CAMECA SX-50 in WDS operative mode at the following conditions: 15 kV excitation voltage, 15 nA beam current, 20 s counting time on peak and 10 s counting time on background, with an electron beam smaller than 2 μm. The standards used were: diopside for Ca (PET) and Mg (TAP), albite for Al and Si (TAP), and pure Sc_2O_3 oxide for Sc (PET). Data reduction was done using the PAP method (Pouchou and Pichoir 1985).

All the Sc-doped samples but pyrope are rather heterogeneous, but the point analyses cluster around different compositions, which are all reported in Table 1. Initial proposed site populations (Table 1) are derived by distributing the total Sc content to complete the occupancy of the "normal" cations (Mg and Ca at the X site, Al at the Y site, and Si at the Z site). In the intermediate compositions, some grains have Sc_2O_3 contents even higher than 5 wt%, suggesting that these compositions are most capable of incorporating Sc, an anomaly which had already been noted during experimental work and atomistic simulation of trace-element behavior (van Westrenen et al. 1999, 2003).

With the exception of the low-Sc crystals in $prp_{60}grs_{40}$, the Ca content is almost constant in each run product from a given nominal composition, and the chemical heterogeneity mainly implies different capability of incorporating Sc at the expenses of ^{X}Mg, ^{Y}Al, and ^{Z}Si. This feature might be also related to slow kinetics of crystallization, which prevents a re-equilibration between the different garnet compositions present in a same run-product. It is also possible that garnet crystallized during quenching; however, these crystals are expected to be extremely small, and would have eluded EMP analysis.

X-rays analysis and structure refinement

Given the small size of the synthetic crystals, single-crystal X-ray analysis could be done only for the Sc-doped pyrope and grossular; their crystal quality was evaluated from the profiles of the diffraction peaks, and the sizes of the selected crystals were $0.10 \times 0.12 \times 0.12$ mm, and $0.03 \times 0.03 \times 0.015$ mm, respectively.

X-ray diffraction data were collected at the maximum resolution allowed by crystal dimensions ($\theta_{max} = 60°$ for pyrope and 40° for grossular) at the CNR-IGG-PV with a Bruker-AXS Smart-Apex CCD-based diffractometer, working with graphite monochromatized Mo$K\alpha$ radiation at 55 kV and 30 mA. Omega rotation frames (scan width 0.2°, scan time 30 s for pyrope and 90 s for grossular, sample-to-detector distance 4 cm) were collected using the SMART software (Bruker-AXS Inc.). Data reduction (including intensity integration, background, Lorentz and polarization corrections) were performed with the SAINT software (Bruker-AXS Inc.). Absorption effects were analytically evaluated by the SADABS software (Sheldrick 1996) and an absorption correction was applied to the data. The unit-cell edge was obtained by the SAINT software after data reduction from least-squares refinements of the centroid of gravity of all the independent reflections with $I_O > 12\sigma(I_O)$, namely 3446 reflections for pyrope (2θ range 8–75°) and of 2108 for grossular (2θ range 12–80°).

The structure refinements (SREF) were done with a program locally developed to deal with complex solid solution (E. Cannillo, personal communication) using scattering factors for fully ionized chemical species. The unweighted full-matrix least-squares refinements were done on F using the reflections with $I > 3\sigma(I)$.

X-ray powder diffraction (XRPD) patterns were recorded for all the synthetic samples in the 2θ range 8–100° (Cu$K\alpha_1$-α_2 radiation), with a step scan of 0.02° and a counting time of 10 s per step using a Siemens D5000 diffractometer operating in Bragg-Brentano geometry. The diffraction patterns were refined with the Rietveld whole-pattern method using the EXPGUI-GSAS software package (Toby 2001; Larson and Von Dreele 1997). The values of the unit-cell edge and of the coordinates of the oxygen atom were refined starting from the SREF values obtained for Sc-doped pyrope and grossular single crystals. The site occupancies were fixed to those obtained by the SREF data for these samples, and to those derived from averaging EMP data for the intermediate garnet compositions. Attempts to refine Sc site occupancies and atomic displacement parameters gave unreliable results.

The details of the single-crystal structure refinement for Sc-doped pyrope and grossular are reported in Table 2. Selected parameters and interatomic distances for all the samples are reported in Table 3, where both single-crystal and powder data are reported for pyrope and grossular to show the general agreement between the two methods. Note that the R factors of the single-crystal and of the Rietveld refinement are on a different scale, and that the latter method is affected by the chemical heterogeneity observed in the run products (Table 1), which broadens the diffraction peaks and thus lowers the overall quality of the refined model.

XAS measurements and data analysis

Samples were prepared by grinding the garnet powders in a mortar to reduce the grain size, mixing them with cellulose and finally pressing them into 5 mm diameter pellets. The Sc K-edge (4492 eV) XAFS data were collected at the beamline ID26 of the European Synchrotron Radiation Facility. ID26 is a high-brilliance insertion-device source equipped with two mirrors for beam focalization and harmonic rejection and a double-crystal monochromator [two flat Si(111) crystals in our experiment]. XANES and EXAFS Sc K-edge spectra were measured in the fluorescence mode using photo-diode detectors. Data acquisition was done in the quick scan mode with synchronous movement of the undulator gap and the Bragg angle of the monochromator. About twenty scans were averaged for each sample.

XANES spectra were analyzed according to standard procedures. The raw XANES spectra were subtracted of the pre-edge background and then normalized on the high-energy side. This normalization procedure takes care of the effects resulting from the different sample thickness and allows comparison of samples with different absorber contents.

The EXAFS signals were extracted from the experimental absorption spectra and analyzed using the interactive program IFEFFIT (Newville 2001) with the support of the graphical utilities ATHENA and ARTEMIS (http://feff.phys.washington.edu/~ravel/software/exafs/).

Phase and amplitude back-scattering functions were calculated using the FEFF8 code (Ankudinov et al. 1998) placing the Sc absorber atoms in the dodecahedrally (X), octahedrally (Y), or tetrahedrally (Z) coordinated crystallographic sites of the garnet structure. The coordination distances were derived from XRD results of the Sc-doped samples. The amplitude reduction factor (S_0^2) was obtained by fitting the Sc K-edge data from the reference compound with known structure (Sc_2O_3). Data from Sc_2O_3, measured in fluorescence mode, were corrected for self-absorption effects (Carboni et al. 2005). The value determined for S_0^2 was 0.6. Multi-shell fits were performed in the R space by minimizing the difference between the raw data and the model EXAFS function.

TABLE 1. Sample codes and unit formulae (based on 12 oxygen atoms) for the samples of this work

Nom. comp.	prp	$prp_{60}grs_{40}$	$prp_{60}grs_{40}$	$prp_{60}grs_{40}$	$prp_{20}grs_{80}$	$prp_{20}grs_{80}$	grs	grs
No. anal.*	(15)	(5)	(7)	(4)	(4)	(5)	(17)	(6)
oxide wt%								
MgO	27.47(33)	15.95(1.17)	19.31(1.46)	15.41(22)	4.24(69)	5.69(38)	–	–
CaO	–	15.47(1.67)	13.02(1.68)	15.60(25)	28.59(1.19)	28.93(14)	34.74(29)	35.18(46)
Al_2O_3	24.61(17)	22.15(8)	22.24(1.6)	21.54(19)	20.80(35)	20.43(42)	20.15(53)	20.44(90)
SiO_2	41.73(51)	40.24(37)	42.07(1.10)	39.41(35)	36.78(9)	39.34(71)	37.25(31)	37.59(28)
Sc_2O_3	6.78(61)	5.70(39)	2.83(1.04)	7.96(46)	8.16(20)	4.96(1.17)	6.73(49)	5.52(27)
Total	100.58(30)	99.52(25)	99.48(29)	99.93(69)	98.56(41)	99.35(30)	98.87(24)	98.72(26)
Unit formulae; Sc distributed to complete the occupancies of the normal cations								
Mg	2.78	1.70	2.03	1.65	0.48	0.63	–	–
Ca	–	1.19	0.98	1.20	2.33	2.31	2.86	2.89
Sc	0.22	0.11	–	0.15	0.19	0.06	0.14	0.11
Al	1.97	1.87	1.85	1.82	1.86	1.80	1.83	1.85
Sc	0.01	0.13	0.15	0.18	0.14	0.20	0.17	0.15
Si	2.83	2.88	2.97	2.83	2.79	2.94	2.86	2.89
Sc	0.17	0.12	0.02	0.17	0.21	0.06	0.14	0.11
Sc total	0.40	0.27	0.17	0.50	0.54	0.32	0.45	0.37

* Number of point analyses performed on each sample and averaged to obtain the reported data.

Discussion

We report in this section the results obtained for the four recycled experimental runs. The presence of other phases could not be detected by either XRPD or SEM analysis. Only two very low-angle reflections (almost at the background level) were observed, but these could not be assigned to any feasible phase. Table 1 shows that all the Sc_2O_3 (5 wt%) added to the four nominal garnet compositions was completely incorporated in the synthesized garnets. Hence, possible crystalline phases not detected by EMP and XRPD analyses, should contain only Mg, Ca, Al and/or Si, and did not invalidate XAS analysis. However, compositional heterogeneity (Table 1) may have prevented a multi-shell fit approach for some of the samples.

Table 2. The results of the single-crystal structure refinements for the Sc-doped samples of this work

Sample	prp	grs
a (Å)	11.4940(5)	11.8830 (9)
θ range	2–60	2–40
no. F_{obs}, $R_{3\sigma}$ (%)	871, 3.67	326, 5.22
no. F_{all}, R_{all} (%)	972, 4.37	383, 5.98
O site:		
ref. occ.	0.80 O^{2-} + 0.20 O	0.80 O^{2-} + 0.20 O
x	0.03290(4)	0.03803(19)
y	0.05061(4)	0.04587(19)
z	0.65349(4)	0.65194(18)
B_{eq} (Å^2)	0.59(1)	0.52(4)
β_{11}	0.00113(2)	0.00095(11)
β_{22}	0.00135(2)	0.00101(11)
β_{33}	0.00089(2)	0.00081(10)
β_{12}	0.00010(2)	0.00017(9)
β_{13}	–0.00015(2)	0.00002(9)
β_{23}	–0.00001(2)	0.00003(9)
T site		
ref. occ.,	0.95(1) Si^{4+} + 0.05 Mg^{2+}	0.95(1) Si^{4+} + 0.05 Sc^{3+}
ref. ss (e)	13.90(2)	14.35(7)
B_{eq}(Å^2)	0.40(2)	0.61(2)
β_{11}	0.00073(2)	0.00096(9)
β_{22}	0.00077(1)	0.00115(6)
Y site		
ref. occ.	1.00(1) Al^{3+} + 0.00 Sc^{3+}	0.93(1) Al^{3+} + 0.07 Sc^{3+}
ref. ss (e)	13.00(8)	13.56(8)
B_{eq} (Å^2)	0.47(1)	0.44(1)
β_{11}	0.00089(1)	0.00079(4)
β_{12}	0.00001(1)	0.00003(6)
X site		
ref. occ.	0.90(1) Mg^{2+} + 0.10 Sc^{3+}	0.95(9) Ca^{2+} + 0.05 Sc^{3+}
ref. ss (e)	12.90(9)	20.05(9)
B_{eq} (Å^2)	0.89(1)	0.51(1)
β_{11}	0.00101(2)	0.00064(5)
β_{22}	0.00202(2)	0.00104(4)
β_{23}	0.00048(2)	0.00023(5)

Comparative structural analysis

In garnets, cation substitutions occurring at a given site strongly affect the size and the geometry of all the other sites; this observation is explained by the extensive edge-sharing between distinct polyhedra (Fig. 1). For instance, the Y-O distance is 1.887 Å in pyrope and 1.925 Å in grossular (CNR-IGG garnet database; first described in Merli et al. (1995), and expanded during the last ten years), although Al is the only octahedral cation in both minerals and the only variable is the site population at the X site. As a consequence, a chemical substitution cannot be deduced from the dimensions of the involved site. Also, the value of the unit-cell edge, which is affected by both chemical substitutions and structural relaxation, has a very complex dependence on composition (Merli et al. 1995; Ungaretti et al. 1995). Therefore, any variation in a given structure parameter must be interpreted by comparison with the trends observed for the distinct garnet solid-solutions.

A plot of the length of the unit-cell edge measured for the samples of this work against the Ca content (Fig. 2) clearly shows the presence of larger cations at the Y and/or at the Z sites. Sc is slightly smaller than Mg, and thus its incorporation at the X site by itself is not expected to increase the *a* value. Notably, Sc-doped pyrope deviates less than Sc-doped grossular from the trend observed for all the natural and synthetic garnets characterized at the CNR-IGG in Pavia.

Figure 3 shows changes in interatomic distances as a function of value of the unit-cell edge. The observed structural changes can be interpreted as follows.

Sc-doped pyrope. The refined X1-O and X2-O distances are slightly longer than in pyrope, but shorter than expected for a = 11.494 Å (Fig. 3a). The O-O edge shared between two X polyhedra (shared X-X) is shorter than expected, whereas the unshared O-O edge (unshared X-X) is roughly in line with the trend. The refined site-scattering value at the X site is 38.7 electrons per formula unit (epfu), showing the presence of significant Sc (~0.30 apfu) substitution for Mg at the X site. The Y-O distance is slightly longer than expected (Fig. 3c), but the refined site-scattering value does not vary from 26.0 epfu, indicating that Sc substitution, if any, is hardly detectable. At

Table 3. Selected results of the structure refinements for the samples of this work

Sample	*a* (Å)	R_{all} %	X1-O (Å)	X2-O (Å)	<X-O> (Å)	Y-O (Å)	Z-O (Å)
prp	11.494(1)	4.4	2.205(1)	2.346(1)	2.275	1.896(1)	1.640(1)
prp*	11.489(1)	5.0	2.205(2)	2.362(2)	2.284	1.885(2)	1.635(2)
$prp_{60}grs_{40}$*	11.649(1)	7.0	2.243(2)	2.397(2)	2.320	1.915(2)	1.650(2)
$prp_{20}grs_{80}$*	11.820(1)	5.0	2.308(2)	2.457(2)	2.382	1.927(2)	1.658(2)
grs	11.883(1)	6.0	2.326(1)	2.488(1)	2.407	1.939(1)	1.650(1)
grs*	11.891(1)	6.5	2.331(2)	2.473(2)	2.402	1.954(2)	1.650(2)

Sample	Sh X-X (Å)	Unsh X (Å)	Sh X-Y (Å)	Unsh Y (Å)	Sh X-T (Å)	Unsh T (Å)
prp	2.711(1)	2.784(1)	2.628(1)	2.732(1)	2.505(1)	2.761(1)
prp*	2.741(2)	2.801(2)	2.625(2)	2.706(2)	2.498(2)	2.753(2)
$prp_{60}grs_{40}$*	2.788(2)	2.828(2)	2.677(2)	2.740(2)	2.528(2)	2.773(2)
$prp_{20}grs_{80}$*	2.916(2)	2.844(2)	2.734(2)	2.715(2)	2.580(2)	2.769(2)
grs	2.961(1)	2.864(1)	2.771(1)	2.714(1)	2.573(1)	2.753(1)
grs*	2.935(2)	2.838(1)	2.786(2)	2.741(2)	2.576(2)	2.751(2)

* Denotes XRPD refinements; Sh = shared; Unsh = unshared; R_{all} SC = $\Sigma|F_o-F_c|/\Sigma|F_o|$; R_{all} Rietveld = $\Sigma|F_o^2-F_c^2|/\Sigma|F_o^2|$.

the Z site, a significant increase in the Z-O bond distance (1.640 vs. 1.633 Å; Fig. 3e) couples with a lower site-scattering value (41.7 vs. 42.0 epfu); this difference is compatible with 0.15 Mg apfu substituting for Si. All this evidence suggests that Sc is incorporated only at the X site in pyrope (and causes a small but significant decrease in size), and that local charge-balance is achieved by incorporation of Mg at the tetrahedral Z site. This coupled substitution implies that a tetrahedron occupied by Mg is coordinated to two dodecahedra occupied by Sc, thus giving rise to clustering effects. The presence of a larger cation at the Z site also explains the longer *a* value measured in Sc-doped pyrope relative to pyrope (11.494 vs. 11.454 Å).

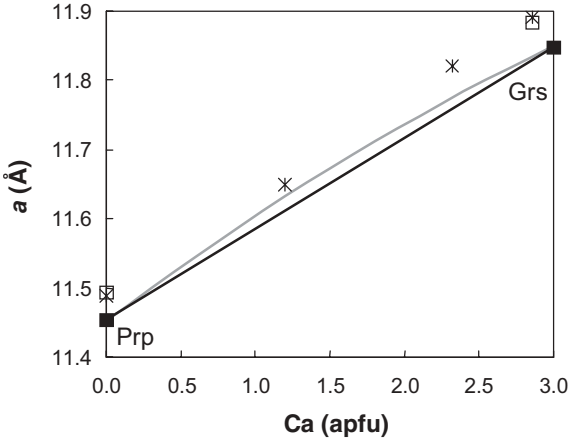

FIGURE 2. The measured values of the unit-cell-edge plotted vs. the Ca content for pure pyrope and grossular (black symbols) and for the samples of this work (empty symbols SREF and crosses XRPD results). In gray the expected behavior along the binary as extrapolated by the CNR-IGG, crystal-chemical database.

Sc-doped grossular. The refined X1-O and X2-O distances are slightly shorter than expected for a sample with a = 11.883 Å (i.e., longer than in grossular, where a = 11.848 Å); again, the shared X-X edge is the most affected (Fig. 3a). The refined site-scattering value at the X site (60.2 epfu) is consistent with up to 0.15 Sc apfu substituting for Ca. The refined Y-O distance is in line with the observed *a* value (Fig. 3c), and couples with a refined site-scattering value of 27.1 epfu (corresponding to 0.14 Sc pfu). The Z-O distance is far longer than expected, even longer than expected for garnets containing variable amounts of larger Z cations (namely, melanites, and solid solutions with schorlomite and kimzeyite; cf. the gray trend pointing toward the upper right angle of Fig. 3e). The refined site-scattering value at the Z site is 43.0 epfu, suggesting 0.15 Sc apfu substituting for Si. The above evidence can be interpreted as a non-selective partitioning of Sc among the three independent structural sites. This result is very peculiar, and certainly warrants further investigation with independent techniques.

The total Sc contents estimated from SREF for Sc-doped pyrope and grossular (0.30 and 0.43 apfu, respectively) are in good agreement with those measured by electron microprobe analysis (0.40 and 0.45 or 0.37 apfu, respectively; Table 1). In the case of Sc-doped grossular, also the site partitioning given in Table 1 is confirmed by SREF. On the contrary, SREF analysis shows that the simplistic site populations proposed for Sc-doped pyrope in Table 1 are not correct. Based on this evidence, a more correct unit formula for the Sc-doped pyrope in Table 1 is $(Mg_{2.61}Sc_{0.39})(Al_{1.97}Sc_{0.01})(Si_{2.83}Mg_{0.17})O_{12}$, which is not electroneutral. Thus, the unit formula most consistent with SREF analysis is $(Mg_{2.70}Sc_{0.30})Al_{2.00}(Si_{2.85}Mg_{0.15})O_{12}$.

An important objection to our interpretation is that the occurrence of Al at the Z site (coupled with that of Sc at the Y site) in Sc-doped

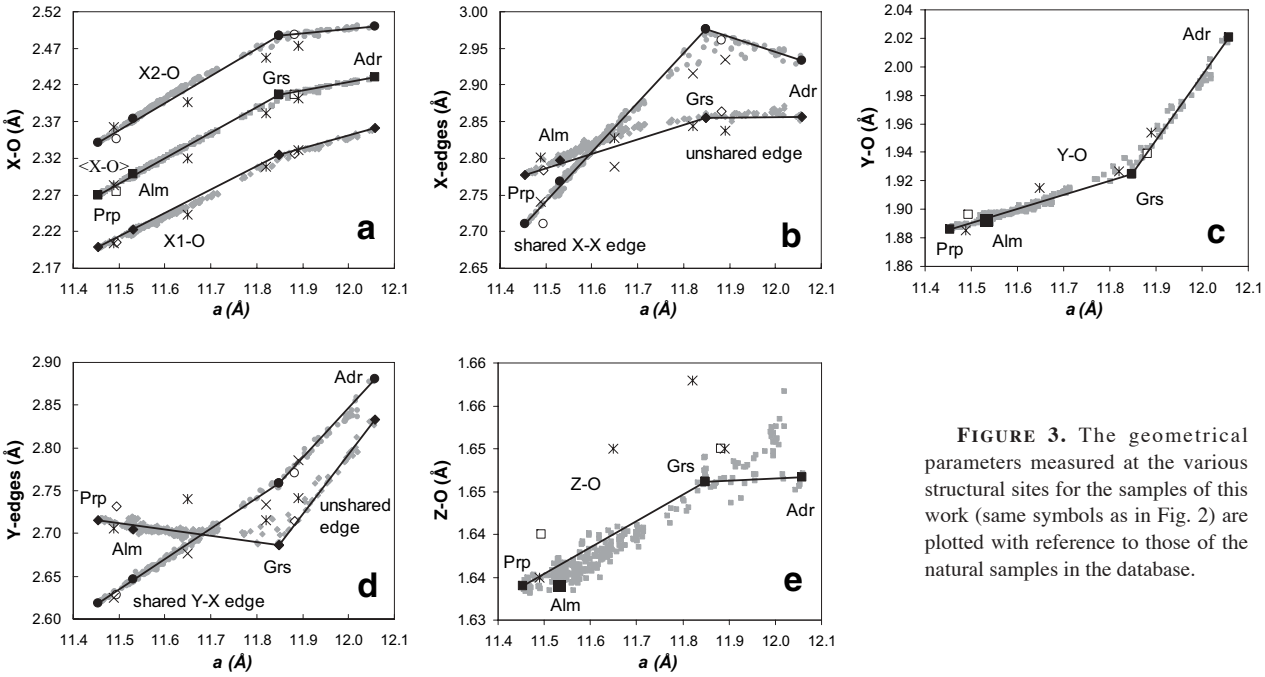

FIGURE 3. The geometrical parameters measured at the various structural sites for the samples of this work (same symbols as in Fig. 2) are plotted with reference to those of the natural samples in the database.

pyrope would apparently be more feasible from a lattice strain point of view than the entrance of Mg. However, we wish to stress that this mechanism is not compatible with the refined bond-lengths and site-scattering values; moreover, it would cause the expansion of one Y and one Z site per each X site occupied by Sc. Therefore, the entrance of one Mg atom at the Z site per two Sc atoms at the X sites actually provides a more favorable relaxation mechanism for the very compact structure of pyrope.

Rietveld refinements were run with fixed site compositions (to those of Table 1), and are not reliable enough to allow a similar interpretation of the structural changes for the solid-solution members. However, they generally confirm that the X sites are smaller (whereas the Y and Z sites are larger) than expected for the measured *a* value, which in turn is longer than expected based on the Ca content. Validation of the hypotheses based on long-range techniques is now left to the analysis and simulation of XAFS data, which is discussed below.

Results of the XANES analysis

Previous XANES investigations done by our group on different elements occurring in garnets (Fe: Quartieri et al. 1993, Ca: Quartieri et al. 1995, Oberti et al. 2006, Yb: Quartieri et al. 1999a, 1999b) have shown that the shape of the XANES spectral features and their relative intensity variations are reliable indicators of local structural changes around the absorbing atom.

The XANES spectra collected at the Sc *K*-edge for the samples of this work are reported in Figure 4; they are ordered from top to bottom as a function of increasing Ca content. Several features are clearly resolved in all the spectra. Notably, the intensities of some peaks, and the shape of the main edge vary strongly with the Ca content of the sample. The behavior shown in Figure 4 implies changes in the local environment of Sc along the series, which may occur either as a function of the composition or of the overall structure. In particular, the general form of the XANES spectra collected on Sc-doped pyrope and grossular are significantly different, suggesting that Sc is present in distinct crystallographic sites.

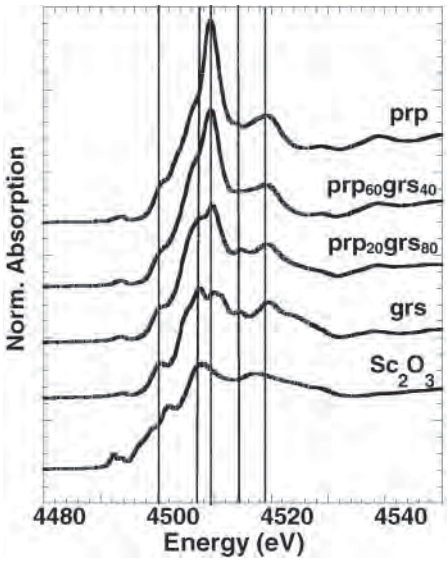

FIGURE 4. XANES spectra collected at Sc *K*-edge. The individual spectra have been normalized with respect to the high-energy side of the curve.

The XANES spectral features of the two solid-solution terms $prp_{60}grs_{40}$ and $prp_{20}grs_{80}$ are more similar to those of the closest end-member. Moreover, they can be reliably simulated by linearly combining the proper percentages of the XANES signals of the two end-members (Fig. 5). The latter evidence suggests that the solid-solution terms have incorporated Sc in several configurations. The spectrum collected on Sc_2O_3, where Sc is in octahedral coordination, has no direct analogies with those of the garnet samples, indicating that Sc cannot exclusively occupy the octahedral site in these garnets.

Results of the EXAFS analysis

The background-subtracted EXAFS data of the Sc-doped garnet samples are shown in Figure 6a, and the corresponding Fourier transforms (*k*-weight = 2; $3.4 < k < 10.5$ Å^{-1}) are shown in Figure 6b. Significant changes can be observed in both the magnitude and positions of the peaks, indicating a different local geometry around Sc. Again, the data collected for samples $prp_{60}grs_{40}$ and $prp_{20}grs_{80}$ are somewhat intermediate, and are more similar to those of the respective end-members.

For Sc-doped pyrope, a multiple-shell fit was done in the *R* space between 1.1 and 3.5 Å with a *k*-range $3.6 < k < 11$ Å^{-1}, using phase and back-scattering functions calculated for Sc absorber atoms occurring at the dodecahedral X site, as suggested by EMPA and XRD analyses. The fit results are given in Table 4 and Figure 7. The fitting parameters were: a unique energy shift (ΔE_0) for all paths; two distinct mean-square displacement values (σ_i^2) for the oxygen shells and the non-oxygen (i.e., Si, Al, and Mg) paths; six independent values of the path length (ΔR_i). Only single-scattering paths were found to contribute significantly to the total EXAFS in the explored range, and their contributions to the model are shown in Figure 7. In the garnet structure, the second shell contribution corresponds to two Z tetrahedra occurring at the same distance. According to the results of the structure refinement, the contribution of the second shell was modeled using one Si atom and one Mg atom (Table 1). The presence of Sc at the Z site can be ruled out by the excellent fit obtained using phase and back-scattering functions calculated for Sc absorber atoms occurring only at the dodecahedral X site. Therefore, the site partitioning obtained by SREF is fully confirmed, and reliable interatomic distances from the Sc absorber are provided (Table 4). In particular, the relative magnitudes of the Sc1-O and Sc2-O distances (2.17 and 2.31 Å, respectively) are consistent with the Mg1-O and Mg2-O distances refined in synthetic pyrope (2.199 and 2.341 Å, respectively).

In a first attempt, the EXAFS signal of Sc-doped grossular

TABLE 4. Fit results for Sc-doped pyrope

	N_{degen}	*R* (Å)	σ_i^2 (Å^2)	<SREF>* (Å)
Sc1 – O	4	2.17(2)	0.001(1)	2.205(1)
Sc2– O	4	2.31(2)	0.001(2)	2.346(1)
Sc – Si	1	2.97(7)	0.004(3)	2.874(1)
Sc – ^{2}Mg	1	3.00(7)	0.004(3)	
Sc – Al	4	3.27(1)	0.004(3)	3.213(1)
Sc – Si	4	3.57(1)	0.004(3)	3.519(1)
Sc – ^{2}Mg	4	3.57(1)	0.004(3)	

* Single-crystal X-ray structure refinement.
Note: $S_0^2 = 0.6$; $\Delta E_0 = 9 \pm 4$; R factor = 0.0010.

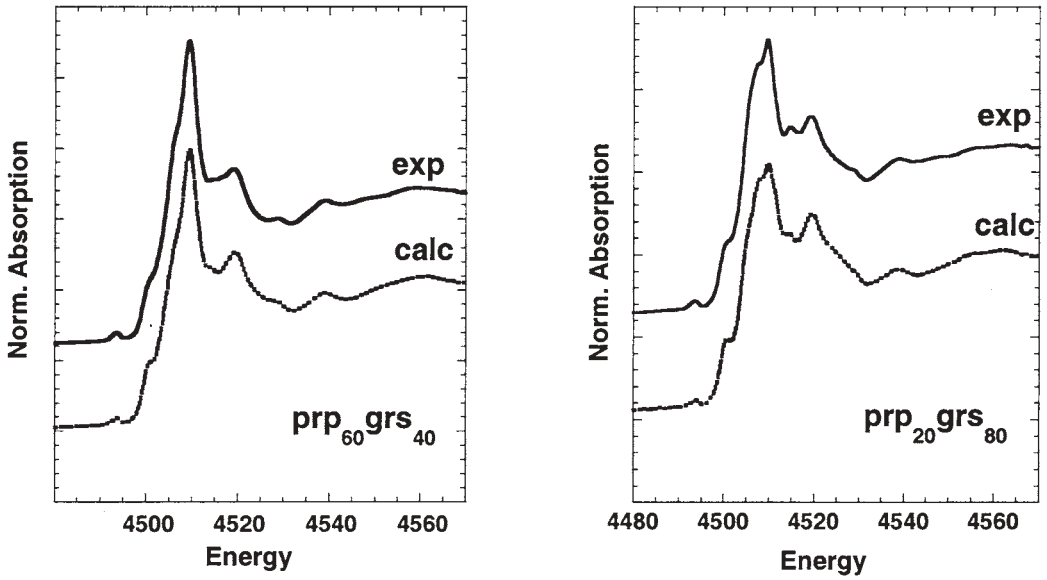

FIGURE 5. Experimental XANES spectra of the solid solutions compared with those simulated by linear combination of the end-member spectra.

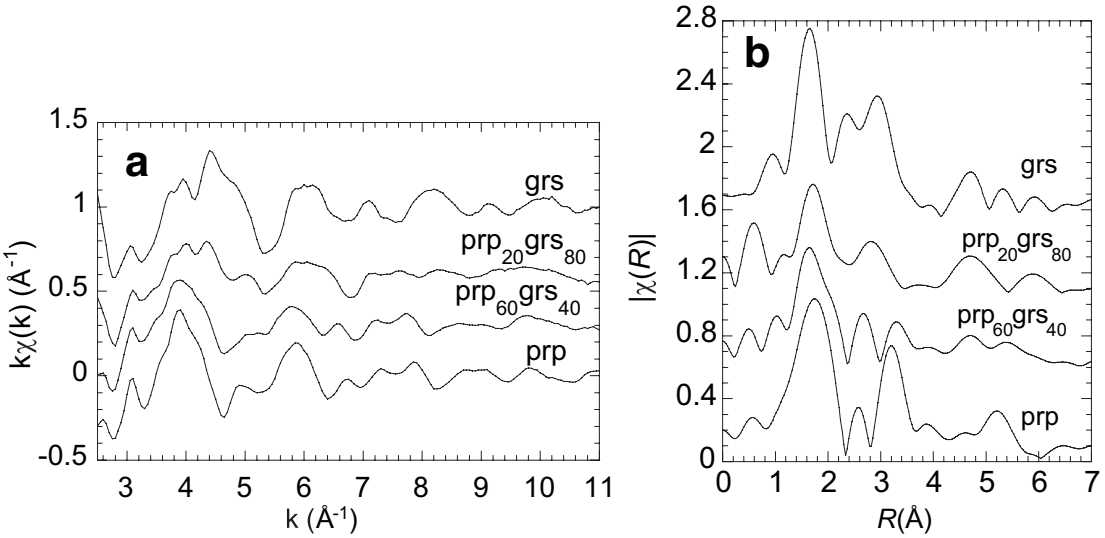

FIGURE 6. (**a**) Sc *K*-edge EXAFS data; (**b**) the corresponding Fourier transforms (k^2, 3.4 < *k* < 10.5 Å^{-1}).

was modeled considering Sc absorber atoms occurring only at the octahedral Y site. This model is in line with previous XRD data on synthetic $Ca_3Sc_2Si_3O_{12}$ (Mill et al. 1977) and XAFS analysis of synthetic solid-solution members covering the join andradite-$Ca_3Sc_2Si_3O_{12}$, which is reported in more detail in the companion paper (Quartieri et al. 2006). The Fourier transforms of the experimental and simulated signals (no fitted sum of paths) obtained for Sc occurring only at the Y site are shown in Figure 8a. The two signals are rather similar, but differences in the relative intensities of the various peaks are clearly visible, especially the peak at an apparent distance of 2.3 Å. Moreover, a multiple-shell fit could not be obtained with this simple model. This failure suggests a more complex distribution of Sc over the different structural sites, as also indicated by the crystal-chemical formula reported in Table 1, in which Sc partitions itself over all the three sites with the following approximate percentages: 40% ^{Y}Sc, 30% ^{X}Sc, and 30% ^{Z}Sc.

The only satisfactory multi-shell fit of the experimental EXAFS signal of Sc-doped grs (Figs. 8b and 8c) was obtained considering the interatomic paths reported in Table 5: six Sc-O paths contributing to the first shell, two Sc-Si (or Sc-Ca) paths contributing to the second shell and three further paths overlapping in a third peak (cf. below for a more detailed discussion). This result must now be interpreted taking into account the complex partitioning of Sc indicated by EMP and SREF analysis. In this scenario, the mean first-coordination shell

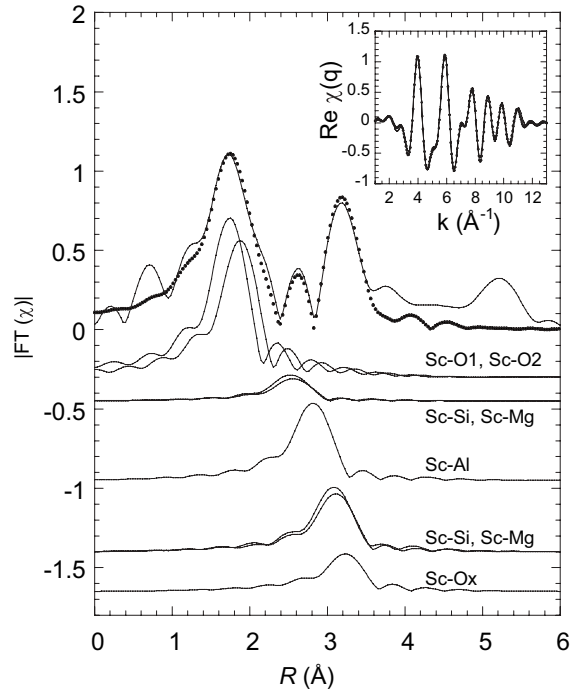

FIGURE 7. Fourier transform of the EXAFS data (solid line) and fit model (dots) for Sc-doped pyrope. In the lower part of the figure, the individual contributions for each single scattering path are shown. The inset reports inverse-Fourier transform of EXAFS data (solid line) and fitted signal (dots).

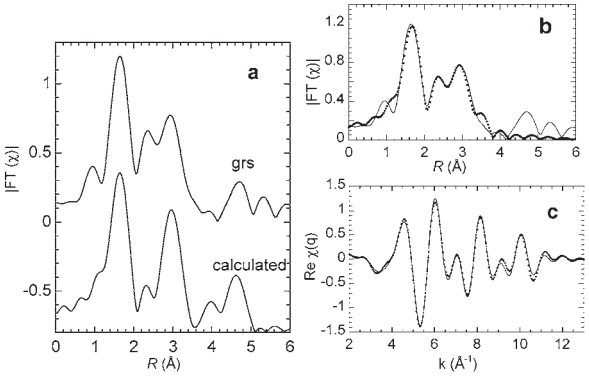

FIGURE 8. (**a**) Fourier transform of EXAFS data for Sc-doped grossular and calculated signal for Sc located only at the Y site (*k*-range: 3.6–11 Å^{-1}). (**b**) Fourier transform of Sc *K*-edge data (solid line) and fitted signal (dots) (*k*-weight = 2); (**c**) inverse-Fourier transform of EXAFS data (solid line) and fitted signal (dots) ($1.1 < R < 2.1$ Å).

TABLE 5. Fit results for Sc-doped grossular

Distance	N_{degen}	*R* (Å)	σ_i^2 (Å^2)
Sc – O	6	2.09(1)	0.004(1)
Sc – Si	2	2.95(2)	0.001(2)
Sc – Ca	6	3.39(1)	0.002(1)
Sc – Si	6	3.39(1)	0.002(1)
Sc – O	6	3.97(1)	0.004(1)

Notes: $S_0^2 = 0.6$; $\Delta E_0 = 6 \pm 2$; R factor = 0.015.

around the absorbing Sc atoms occurring at the three distinct sites results from the sum of: 40% ^{Y}Sc contributing with (0.4 × 6) = 2.4 oxygen atoms, 30% ^{X}Sc contributing with (0.3 × 8) = 2.4 oxygen atoms, and 30% ^{Z}Sc contributing with (0.3 × 4) = 1.2 oxygen atoms. The resulting total number of oxygen atoms surrounding the Sc absorber is therefore 6, which is exactly the coordination number reported in Table 5 for the first-shell fit. The value obtained from the fit for the first shell inter-atomic distance (2.09 Å) can be evaluated on the basis of the estimated bond distances of Sc in the three distinct sites. We can use for ^{Y}Sc the Sc-O bond distance found by Quartieri et al. (2006) in Sc-andradites (i.e., 2.06 Å), and for ^{X}Sc the average of the two Sc-O distances measured in Sc-doped prp (2.24 Å; this work). No experimental data are available for ^{Z}Sc-O, and no estimate of the ionic radius in fourfold coordination is reported; however we can reasonably predict a distance in the range 1.9–2.0 Å based on the atomic radius and its relations with Al. The value obtained from the first shell fit is largely justifiable based on these distinct Sc-O bond distances.

The second peak in the Fourier Transform of Figure 8b was fitted using two Sc-Si (or Sc-Ca) paths with a distance of 2.95 Å. This local arrangement is roughly compatible with the presence of 30% ^{X}Sc (contributing with 0.3 × 2 = 0.6 Si or Ca at about 3 Å) and 30% ^{Z}Sc (contributing with 0.3 × 2 = 0.6 Ca at 3.06 Å), which gives a total expected coordination number of 1.2. However, given the complexity of the atomic interactions, the results of the second-shell fit can be considered in a satisfactory agreement with the proposed model of Sc partitioning.

Finally, the third peak of the Fourier Transform of Figure 8b was fitted combining three paths corresponding to 6 Ca + 6 Si atoms at about 3.4 Å and 6 O atoms at about 3.9 Å. This configuration corresponds to that of Sc at the Y site (Mill et al. 1977), but is also compatible with the higher coordination shells of Sc occurring at the other two sites. However, it was impossible to explicitly include all the paths originating from sites X and Z in the fit because this would have generated an unacceptably high number of fitting parameters.

In conclusion, the non-conventional fitting procedure discussed below provides EXAFS results consistent with both chemical and crystallographic data, and confirms the Sc partitioning in grossular.

The solid-solutions $prp_{60}grs_{40}$ and $prp_{20}grs_{80}$ have more complex Fourier transform features, although the overall shapes resemble those of the end-members. Based on the EXAFS results obtained on Sc-doped grs and on the analysis of the XANES spectra, Sc is also expected to partition over more sites in the solid solutions. However, the observed chemical heterogeneity and the lack of precise information on the true local geometry of the major cations in the solid-solution make a multiple-shell fit of the EXAFS data infeasible.

CONCLUDING REMARKS AND IMPLICATIONS ON MODELING

The first multi-technique study of Sc incorporation in garnets belonging to the pyrope-grossular join has provided long-range and short-range evidences for a multifarious incorporation scheme, which mainly depends on the garnet overall composition. Although the chemical heterogeneity of the intermediate samples prevented their detailed crystal-chemical description

and spectroscopic analysis, an EXAFS multi-shell fit was done on the two Sc-doped end-members, allowing the quantitative description of the geometry of the Sc local environment. In Sc-doped pyrope, where the structure is kept tight by the presence of small dodecahedral sites occupied by Mg (0.89 Å), Sc (0.87 Å) enters only the X site. Sc incorporation at the Y site, which shares six out of its twelve O-O edges with six adjacent X sites, is therefore prevented. The incorporation of one Mg atom at the tetrahedral Z site (which balances for 2 Sc atoms at the 2 adjacent X sites) is preferred to that of Sc in a ratio 1:1 because of the smaller overall increase in size. Actually, ionic radii for Sc and Mg in tetrahedral coordination are not available, but Sc is larger than Mg in octahedral coordination (0.745 vs. 0.72 Å).

The Sc1-O and Sc2-O distances at the X site have been reliably estimated by EXAFS analysis; their values [2.17(2) and 2.31(2) Å, respectively] are in the correct relation with respect to the Mg1-O and Mg2-O distances refined in synthetic pyrope, i.e., 2.199(1) and 2.341(1) Å. The X and the Y sites relax because of the presence of a larger cation (Mg) at the Z site (X-O = 2.275 vs. 2.270 Å, Y-O = 1.896 vs. 1.886 Å), which also lengthens the shared X-Z edges (2.505 vs. 2.496 Å).

When the presence of some Ca at the X site relaxes the garnet structure, Sc can enter all the three independent sites and assume three distinct coordination environments. Interestingly, octahedral Sc never exceeds 0.20 apfu in all compositions tested. This evidence may suggest a structural constraint on the enlargement of the Y octahedron in the garnet structure when the dominant cation is Al. According to this hypothesis, there is no limit to the (ideal) incorporation of Sc at the Y site along the join andradite-$Ca_3Sc_2Si_3O_{12}$, where it substitutes for Fe^{3+} (0.645 Å) (Quartieri et al. 2006). However, the local environment of octahedral Sc is virtually constant (Sc-O ~ 2.1 Å) in all the garnet compositions for which information is available.

The implications of this study on natural systems (which always contain other chemical constituents, the most relevant of which are Li, Na, and also Fe) cannot be discussed straightforwardly. However, this work provides at least three hints of interest for models of trace-element behavior in garnets.

The first hint obviously is that Sc can in principle be incorporated at different sites, the site preference being a function of the overall garnet chemistry; this conclusion explains the positive deviation of D_{Sc} from the ideal fit for trivalent cations at the X site observed by van Westrenen et al. (1999) in Ca-rich garnets. The second hint is that intermediate solid-solution members have a higher compliance toward the incorporation of higher trace-element contents, such as trivalent cations at the X site (Sc and also REE, as already found by van Westrenen et al. 1999, 2001, who also modeled the lowest E_X values for intermediate compositions). This finding is in line with the many non-ideal properties of the pyrope-grossular solid-solution, and could be related to the presence of a particular strain when the X sites are almost equally occupied by small (Mg, Fe, Sc) or large (Ca) cations. The third hint is that local charge balance after incorporation of two trivalent cations into two X dodecahedra can be obtained also by substitution of a divalent cation at the bridging Z tetrahedron. All these conclusions add further interest to atomistic simulations of the garnet solid solutions.

ACKNOWLEDGMENTS

This work benefited from the contribution of many persons, who are all warmly thanked for their help. Andrea Orlando (CNR-IGG, Firenze) prepared the starting materials for the synthesis of Sc-doped garnets, and Detlef Krauße (Bayerisches GeoInstitut, Bayreuth) assisted during electron microprobe analysis. Funding for the project was provided by the MIUR-COFIN grant "Geo-crystal-chemistry of trace elements." G.I. run the syntheses during the post-doc stay of G.I. at the Bayerisches GeoInstitut, Bayreuth, supported by a Sofja Kovalevskaja Award to Tiziana Boffa-Ballaran.

We also wish to thank Wim van Westrenen and George Lager for their careful and constructive comments.

REFERENCES CITED

Ankudinov, A.L., Ravel, B., Rehr, J.J., and Conradson, S.D. (1998) Real space multiple scattering calculation of XANES. Physical Reviews B, 58, 7565–7576.

Blundy, J.D. and Wood, B.J. (1994) Prediction of crystal-melt partition coefficients from elastic moduli. Nature, 372, 452–454.

Brice, J.C. (1975) Some thermodynamic aspects of the growth of strained crystals. Journal of Crystal Growth, 28, 249–253.

Carboni, R., Giovanni, S., Antonioli, G., and Boscherini, F., (2005) Self-absorption correction strategy for fluorescence-yield soft X-ray near edge spectra. Physica Scripta, T115, 986–990.

Ganguly, J., Cheng, W., and O'Neill, H.St.C. (1993) Syntheses, volume and structural changes of garnets in the pyrope-grossular join: implications for stability and mixing properties. American Mineralogist 78, 583–593.

Ito, J. and Frondel, C. (1968) Synthesis of the Sc analogue of aegirine, spodumene, andradite, and melanotekite. American Mineralogist, 33, 1276–1280.

Larson, A.C. and Von Dreele, R.B. (1997) GSAS: General Structure Analysis System. Document LAUR 86-748, Los Alamos National Laboratory.

Merli, M., Callegari, A., Cannillo, E., Caucia, F., Leona, M., Oberti, R., and Ungaretti, L. (1995) Crystal-chemical complexity in natural garnets: structural constraints on chemical variability. European Journal of Mineralogy, 7, 1239–1249.

Mill, B.V., Belokoneva, E.L., Simonov, M.A., and Belov, N.V. (1977) Refined crystal structures of the scandium garnets $Ca_3Sc_2Si_3O_{12}$ and $Cd_3Sc_2Ge_3O_{12}$. Zhurnal Strukturnoi Khimii, 18, 399–402.

Newville, M. (2001) IFEFFIT: interactive XAFS analysis and FEFF fitting. Journal of Synchrotron Radiation, 8, 322–324.

Oberti, R., Quartieri, S., Dalconi, M.C., Boscherini, F., Iezzi, G., and Boiocchi, M. (2006) Distinct local environments for Ca along the non-ideal pyrope-grossular solid-solution: a new model based on crystallographic and EXAFS analysis. Chemical Geology, 335, 347–359.

Pouchou, J.L. and Pichoir, F. (1985) "PAP" $\phi(\rho Z)$ procedure for improved quantitative microanalysis. In J.T. Armstrong, Ed., Microbeam Analysis, p. 104–160. San Francisco Press, California.

Quartieri, S., Antonioli, G., Lottici, P.P., and Artioli, G. (1993) X-ray absorption spectroscopy investigation at the Fe K-edge of natural garnets from Ivrea Verbano zone. Mineralogical Magazine, 57, 249–256.

Quartieri, S., Chaboy, J., Merli, M., Oberti, R., and Ungaretti, L. (1995) Local structural environment of calcium in garnets: a combined structure-refinement and XANES investigation. Physics and Chemistry of Minerals, 22, 159–169.

Quartieri, S., Antonioli, G., Geiger, C.A., Artioli, G., and Lottici, P.P. (1999a) XAFS characterization of the structural site of Yb in synthetic pyrope and grossular garnets. Physics and Chemistry of Minerals, 26, 251–256.

Quartieri, S., Chaboy, J., Antonioli, G., and Geiger, C.A. (1999b) XAFS characterization of the structural site of Yb in synthetic pyrope and grossular garnets. II: XANES full multiple scattering calculations at the Yb L_I- and L_{III}-edges. Physics and Chemistry of Minerals, 27, 88–94.

Quartieri, S., Boscherini, F., Chaboy, J., Dalconi, M.C., Oberti, R., and Zanetti, A. (2002) Characterization of trace Nd and Ce site preference and coordination in natural melanites: a combined X-ray diffraction and high-energy XAFS study. Physics and Chemistry of Minerals, 29, 495–502.

Quartieri, S., Dalconi, M.C., Boscherini, F., Oberti, R., and D'Acapito, F. (2004) Crystal-chemistry of trace Rare Earth Elements in garnets by high-energy XAFS: new data on the site geometry of dysprosium. Physics and Chemistry of Minerals, 31, 162–167.

Quartieri, S., Oberti, R., Boiocchi, M., Dalconi, M.C., Boscherini, F., Safonova, O., and Woodland, A.B. (2006) Site preference and local geometry of Sc in garnets: II. The crystal-chemistry of octahedral Sc in the andradite-$Ca_3Sc_2Si_3O_{12}$ join. American Mineralogist, 91, 1240–1248.

Shannon, R.D. (1976) Revised effective ionic radii and systematic studies of interatomic distances in halides and chalcogenides. Acta Crystallographica, A32, 751–767.

Sheldrick, G.M. (1996) *SADABS*. Siemens Area Detector Absorption Correction Program. University of Göttingen, Germany.

Toby, B.H. (2001) EXPGUI, a Graphical User Interface for GSAS. Journal of Applied Crystallography, 34, 210–213.

Ungaretti, L., Leona, M., Merli, M., and Oberti, R. (1995) Non-ideal solid-solution in garnet: crystal-structure evidence and modelling. European Journal of Mineralogy, 7, 1299–1312.

van Westrenen, W., Blundy, J.D., and Wood, B.J. (1999) Crystal-chemical controls on trace-element partitioning between garnets and anhydrous silicate melts. American Mineralogist, 84, 838–847.

van Westrenen, W., Allan, N.L., Blundy, J.D., Purton, J.A., and Wood, B.J. (2000) Atomistic simulation of trace element incorporation into garnets—comparison with experimental garnet-melt partitioning data. Geochimica et Cosmochimica Acta, 64, 1629–1639.

van Westrenen, W., Wood, B.J., and Blundy, J.D. (2001) HFSE/REE fractionations during partial melting in the presence of garnet: implications for identifications of mantle heterogeneities. Geochemistry Geophysics Geosystems, 2, paper 2000GC00133.

van Westrenen, W., Allan, N.L., Blundy, J.D., Lavrentiev, M. Yu., Lucas, B.R., and Purton, J.A. (2003) Dopant incorporation into garnet solid solutions—a breakdown of Goldschmidt's first rule. Chemical Communications, 786–787.

Woodland, A.B. and Angel, R.J. (1996a) Incorporation of Sc in garnet and the properties of $Ca_3Fe_2Si_3O_{12}$-$Ca_3Sc_2Si_3O_{12}$ garnet solid solutions. EOS Transactions of the American Geophysical Union, 77, F829.

——— (1996b) Synthesis and properties of $Ca_3Fe_2Si_3O_{12}$-$Ca_3Sc_2Si_3O_{12}$ garnet solid solutions. Terra Absracts, 8, 68.

MANUSCRIPT RECEIVED JULY 18, 2005
MANUSCRIPT ACCEPTED MARCH 30, 2006
MANUSCRIPT HANDLED BY MARC HIRSCHMANN